A STUDY INTO THE EFFECTS OF GAS FLOW INLET DESIGN OF THE RENISHAW AM250 LASER POWDER BED FUSION MACHINE USING COMPUTATIONAL MODELLING

A.M. Philo[1, 3], C.J. Sutcliffe [2, 3], S.Sillars[1, 3], J. Sienz[1], S.G.R. Brown[1], N.P. Lavery[1]

[1] College of Engineering, Swansea University, Bay Campus, Crymlyn Burrows, Swansea, SA1 8EN, UK

[2] Department of Engineering, University of Liverpool, Brownlow Hill, Liverpool, L69 3GH, UK

[3] Renishaw plc, Additive Manufacturing Products Division, Brooms Road, Stone Business Park, Stone, Staffordshire, ST15 0SH, UK

Abstract

Previous work has highlighted the importance of the gas flow system in laser powder bed fusion (L-PBF) processes. Inhomogeneous gas flow experienced at the surface of the powder bed can cause variations in mechanical properties over a build platform, where insufficient removal of by-products which cause laser attenuation and redisposition of by-products are believed to contribute to these variations. The current study analyses the gas flow experienced over a build platform in a Renishaw AM250 metal powder bed fusion machine via Hot Wire Anemometer (HWA) testing. Velocity profiles of the flow directly above the powder-bed and through the centre plane normal to the inlets have been categorized. These HWA results illustrate the inhomogeneity of the gas flow experienced over the build platform and from literature imply that there will be insufficient removal of by-products and hence variable build quality in specific areas of the build platform.

A Computational Fluid Dynamics (CFD) model was created in ANSYS Fluent and validated against HWA results coupled with a Discrete Phase Model (DPM) representing the expulsion of spatter. Velocity contours of simulated against experimental are compared, where the results appear in good agreement.

The multiphase CFD model was then used to explore the effects of changing inlet design parameters using a Design of Experiments (DOE) study based on an Optimal Space Filling (OSF) method. This was to understand the effect of design parameters on flow uniformity, local gas velocity over the processing area and spatter particulate accumulation within the build chamber. The initial design study found that flow uniformity could potentially be increased by 21.05% and spatter accumulation on the processing area could be reduced by 26.64%. In addition, this has given insight into important design considerations for future generation of L-PBF machines.

1. Introduction

Additive layer manufacturing (ALM) is a rapidly developing process, with origins in rapid prototyping which is attracting end-users in aerospace, automotive, medical and other sectors. There have been many processes developed in this field such as electron beam freeform fabrication (EBF^3), wire + arc and laser powder bed fusion (L-PBF). In the work presented we are interested in L-PBF which is alternately known as selective laser melting (SLM), selective laser sintering (SLS), direct metal laser sintering (DMLS) and electron beam melting (EBM). L-PBF allows for the fabrication of small intricate components from melting or sintering of a metal powder, using a high powered laser, and creating a three dimensional object on a layer-by-layer basis. In addition, L-PBF provides a useful tool creating fully dense parts across a range of metal alloys.

The process of L-PBF is extremely complicated; involving a range of multi-physical coupled processes including energy absorption, heat transfer, fluid flow and thermo-capillary convection which make the process particularly challenging when modelling. Many of the physical phenomena inherent in L-PBF are influential on the properties of the end product. Das [1] identifies some of the important physical mechanisms in laser sintering of metals where the importance of having a ultrahigh purity inert gas or high vacuum environment to ensure inter-layer bonding and wetting is discussed . Therefore, understanding these effects based on the input parameters is important.

Modelling has been utilised to understand the effects of such physical aspects throughout powder based additive manufacturing processes. King et al [2] give a review of modelling and simulation used in the L-PBF process and highlight its importance for understanding of the fundamental physics involved in the process. They highlight the importance of powder scale models as a tool for certifying fabricated parts. Due to the complex multi-physical nature of such processes simplifications have to be made. Fu and Guo [3] use a three dimensional finite element conduction model to simulate multiple-layer depositions for Ti-6Al-4V of the SLM process to understand the influence of process parameters without modelling complicated computationally intensive multi-physics. They found that melt pool geometries compared with experimental data with reasonable accuracy. Korner et al. [4] use a 2D lattice Boltzmann model (LBM) to simulate the EBM process to investigate melting and re-solidification of a randomly packed powder bed to demonstrate the effect of process parameters. They highlighted the importance of powder packing on the melt pool characteristics.

Generally more complex physical models which incorporate fluid flow and vaporisation models have been underdeveloped due to high computational expense. However, recently more complex physical models are being modelled due to recognition of the importance of such physical effects. Khairallah et al. [5] created a mesoscopic powder scale model which predicts and demonstrates the effects of recoil pressure and Marangoni convection in the L-PBF process by utilising large scale supercomputers. The model demonstrated reveals the formation mechanisms of pores, spatter and the denudation zone and outlines how these are generated and ways in which to avoid them. Lee and Zhang [6] simulate powder packing based on the discrete element method coupled with a three dimensional heat and fluid flow model for L-PBF for a Ni-base super alloy, IN718, where they use the model to assess the solidification morphology and grain size of the material where they found that the morphology of the microstructure was predominately columnar with some cellular structures where modelling and experimental results were in good agreement. They concluded that the 3D transient heat transfer and fluid flow model is limited to side-by-side laser scans due to such high computational cost. Mindt et al. [7] simulate the first step of the L-PBF process; coating of the processing area. They simulate spreading of commercial Ti-6Al-4V powder using the discrete element method then predict

melt pool geometries using a numerical thermal model. They found that inhomogeneity of the coated powder can lead to increased surface roughness.

In addition, larger scale models which investigate a macroscale level of analysis have been undertaken. Hussein et al. [8] use a three dimensional finite element simulation to investigate temperature and stress fields in single 316L stainless steel layers built without-support and found that cracks found in overhang layers initiate in areas of compressive stress. They then used this model to add supports to regions which require them. Whilst Roberts et al. [9]investigate multiple layers in the L-PBF process for the prediction of residuals stresses using what is known as an element birth and death technique finding that this technique was in good agreement with experimental results.

However, there has been limited published literature on the effects of the shielding gas flow system to the L-PBF process. The shielding gas flow is used in the L-PBF processes mainly to provide an inert atmosphere reducing reactive gas pick-up by the liquid metal largely against oxidisation and nitration which is particularly prevalent during the production of aluminium alloys. It is also used as a tool to remove process by-products from the process zone. These by-products primarily form from the melting and vaporisation of the metal powder which causes a welding plume; this can disturb the laser and can also cause formation of nano-scale particles from rapid condensation of this weld plume. In addition, ejected particles and ejected liquid particles, known as spatter, can occur due to weld pool instabilities. The extent to which the importance and relevance of the removal of by-products from the process zone is becoming more apparent. Ladewig et al. [10] studied the effect of the gas flow system on the width of single welds in the L-PBF process using an EOS Eosint M280 machine. They discovered that if the local flow velocity is too low then the probability of re-deposition of by-products is much higher as well as attenuation of the laser by the welding plume. They concluded that both of these effects can lead to balling which causes incomplete fusion within the material.

Liu et al. [11] presented the effect of spatter on the mechanical properties of AISI 316L stainless steel. They performed single line experiments using a high speed camera to analyse spatter behaviour where they found that the amount of energy inputted to the system affects the size, scattering state and jetting height of the recorded spatter. They then performed tensile testing of spatter contaminated powder against uncontaminated powder and found that the spatter contaminated powder yielded significantly poorer tensile strength in comparison to the uncontaminated powder. Ferrar et al. [12] demonstrated that the flow of argon in the gas flow system has a significant effect on the porosity and strength of as built parts and concluded that a uniform flow distribution is essential for component homogeneity across a build platform and for optimal build quality.

Ding et al. [13] showed that a local shielding device in wire + arc additive layer manufacturing caused three orders of magnitude improvement of contamination levels of oxygen below 2000 ppm and showed that mechanical properties (hardness) were not affected as long as the level was below 4000 ppm. In addition, Masmoudi et al. [14] created a multiphase CFD model to understand the laser-material-atmosphere interaction to understand the effect of process parameters and protective gas pressure on the spatial thermal distribution in the process where they showed that a decrease of pressure gave ruse to a strong expansion of the metal vapour in the interaction region of their model.

The purpose of the work presented was to:

- Define the gas flow in the Renishaw AM250 metal powder bed fusion machine.
- Create a robust and reliable 3D CFD model of the current design configuration.

- Perform simple and realistic design changes to analyse whether the gas flow experienced over the process zone can be improved.

The aims for the optimisation were to meet the following criterion:

- Improve the gas flow uniformity over the entire processing area.
- Reduce the amount of spatter particulates accumulating over the processing area.

To perform such an investigation experimentally would be time-consuming and expensive. A validated CFD model gives the user certain freedom and a degree of confidence in performing design iteration changes at low cost in comparison to experiment, and allows for much less restricted investigations.

2. Experimental gas flow testing

A hot wire anemometer (Airflow TA 465 Series, UK) was used to categorise the flow field within the AM250 chamber. A Perspex screen was mounted to the front of the machine where a series of holes for insertion of the HWA probe were created. During readings the remainder of the holes were closed to reduce the amount of leakage. To categorise the processing area, 0.271 m^2 , a series of measurements with 6 holes along the width with 50 mm intervals and 11 depths of 0.25 mm intervals were recorded as shown in Figure 1.
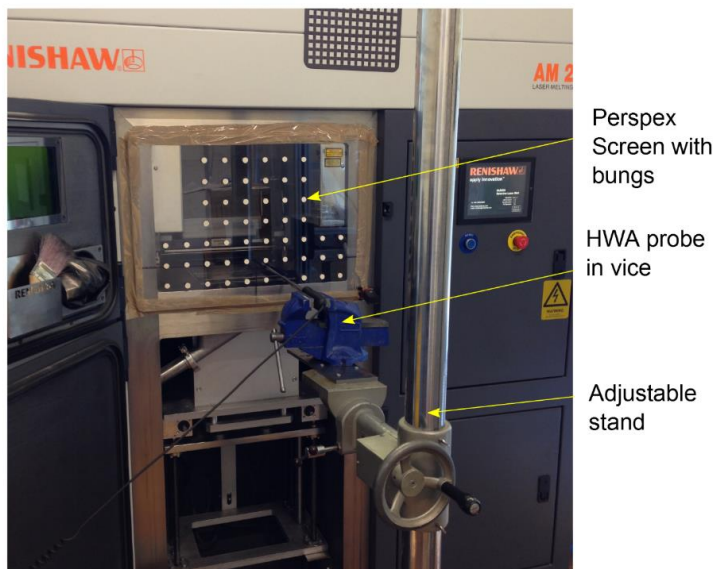

Figure 1: Hot wire anemometer testing set up

This resulted in 66 readings per plane. These readings were recorded over 20 second intervals per reading with the manufacturer's accuracy of $\pm3\%$ or ±0.015 m/s error; whichever is greater. In addition, a 2 minute break after consecutive readings was allowed for the flow to settle. Readings were taken approximately 3 mm above the base plate as close as the probe allowed and in the normal plane to the gas flow inlets.

During an actual build the chamber is first vacuumed and then filled with argon to create an inert atmosphere. In this work air was chosen to categorise the flow field. As argon and air have similar densities 1.622 and 1.225 kg/m^3, respectively, this difference would have minimal effect on the fluid flow properties; namely turbulence regimes and compressibility. Air was used instead of argon during testing due to health and safety; as there was a possibility of some

leakage from the access ports. Additionally, using air allowed the experimental gas to remain constant as there would not be a mixture of fluids. The set-up of the experimental procedure is shown in Figure 1 and the results of the contour plots of the different planes are shown in Figure 2.
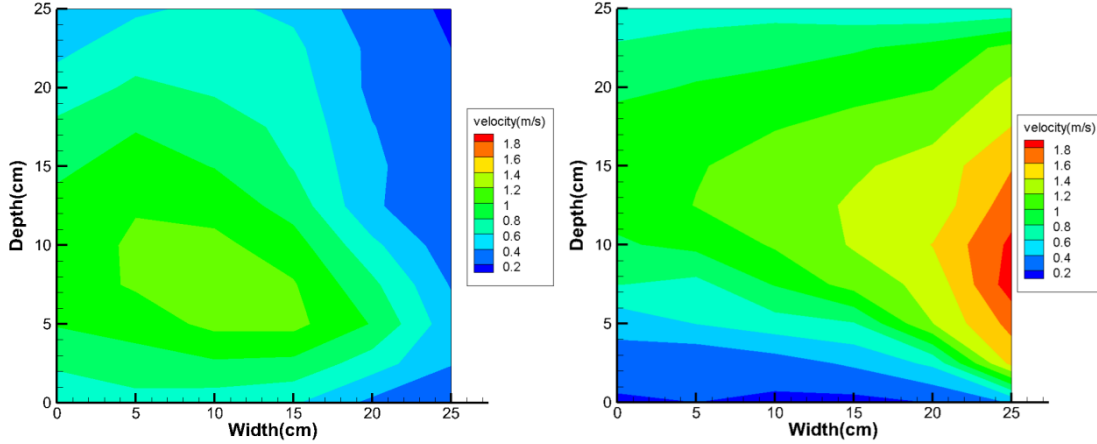

Figure 2: 2D contour plots of velocity (m/s) centre plane: normal to the direction of the inlets b) powder-bed 3mm above baseplate at standard 15Hz pump setting

3. Computational Model

The fluid flow model which used the CFD software package ANSYS Fluent was three dimensional, incompressible and turbulent. In addition, the model was assumed to be in steady state as experimental results did not show any time dependent features. The equations for continuity and momentum can be described as the following

$$\frac{\partial u_i}{\partial x_i} = 0 \tag{1}$$

$$\rho u_j \frac{\partial u_i}{\partial x_j} = \frac{\partial \tau_{ij}}{\partial x_j} - \frac{\partial p}{\partial x_i} \tag{2}$$

Where ρ is the density, u is the velocity, p is pressure and τ the deviatoric stress, expressed as:

$$\tau_{ij} = \mu \left(\frac{\partial u_i}{\partial x_j} + \frac{\partial u_j}{\partial x_i} \right) \tag{3}$$

Where μ is the molecular viscosity coefficient and the subscripts i and j represent the directions in a 3D Cartesian coordinate system.

The Reynolds number was calculated based on the diameter of a single jet of 0.012 m as the characteristic length scale and an estimated jet velocity of be 5 m/s. On this basis, the Reynolds number was found to be in the order of 4000 placing the flow in the turbulent or transitional regime. Literature was reviewed to find the most appropriate turbulence model before model development was undertaken. Oberkampf and Trucano [15] give a fundamental strategy for verification and validation of CFD models which helped guide model development. Then after testing of the most appropriate turbulence models in the model development stage a $\kappa - \epsilon$ realizable turbulence model with Menter-Lechner wall functions was found to be most

appropriate. The $\kappa - \omega$ SST similarly gave good results. However, with the need for refinement near the walls, increasing the total amount of elements, and for slower convergence the $\kappa - \epsilon$ realizable turbulence model was chosen. This model is most accurate for flows in the far field zones, which is applicable for this scenario and found through thorough testing of the most appropriate turbulence models.

3.1 Boundary conditions

The inlet was defined by a mass flow rate at the beginning of the inlet rail. The mass flow rate, $\dot{m}$, was calculated through the volumetric flow rate of the closed loop gas flow system which was set to 15 m³/hr giving a mass flow rate of 0.0051 kg/s for air. The outlet was defined to be an outflow where mass is conserved in the closed loop system. Figure 3 shows the geometry of the fluidic region where boundary locations have been indicated in addition to HWA readings planes and reading line locations. Table 1 highlights the boundary conditions and fluid flow parameters.

Table 1: Boundary conditions and fluid flow parameters

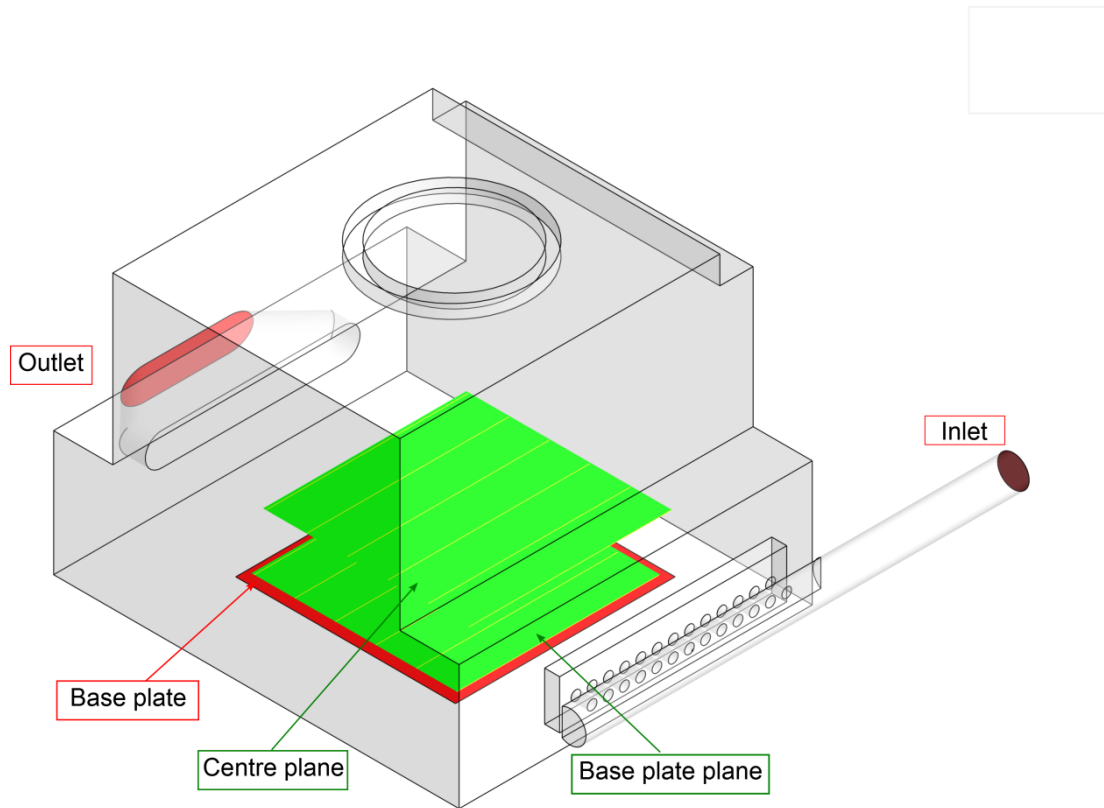| Property	Symbol	Value	Units	Source
Density	ρ	1.225	kg/m³	ANSYS
Dynamic viscosity	μ	1.789 x 10^{-5}	kg/(ms)	ANSYS
Diameter of single jet	D	0.012	m	Measured
Estimated maximum velocity for single jet	V	5.0	m/s	Calculated
Reynolds number*	Re	4108	N/A	Calculated
Mass flow rate	$\dot{m}$	0.0051	kg/s	Calculated

*based on diameter of a single jet

Figure 3: Geometry definition and identification of two HWA reading planes (green) with HWA reading line locations (yellow)

3.2 Mesh

The mesh used for simulations utilised the Cut Cell cartesian assembly meshing method in ANSYS workbench, which offers a nearly purely hexahedral element grid; which is indeed preferable for CFD simulations. Figure 4 shows the 3D shell mesh used for simulations. For the baseline model, 8 computational grids ranging from approximately 300,000 to 7,000,000 elements were used to find mesh independence of velocity values. A grid of 2,700,113 elements was found to be sufficient for accuracy. For all subsequent case study simulations roughly the same amount of elements were used, small variations occurred due to small geometrical modifications.
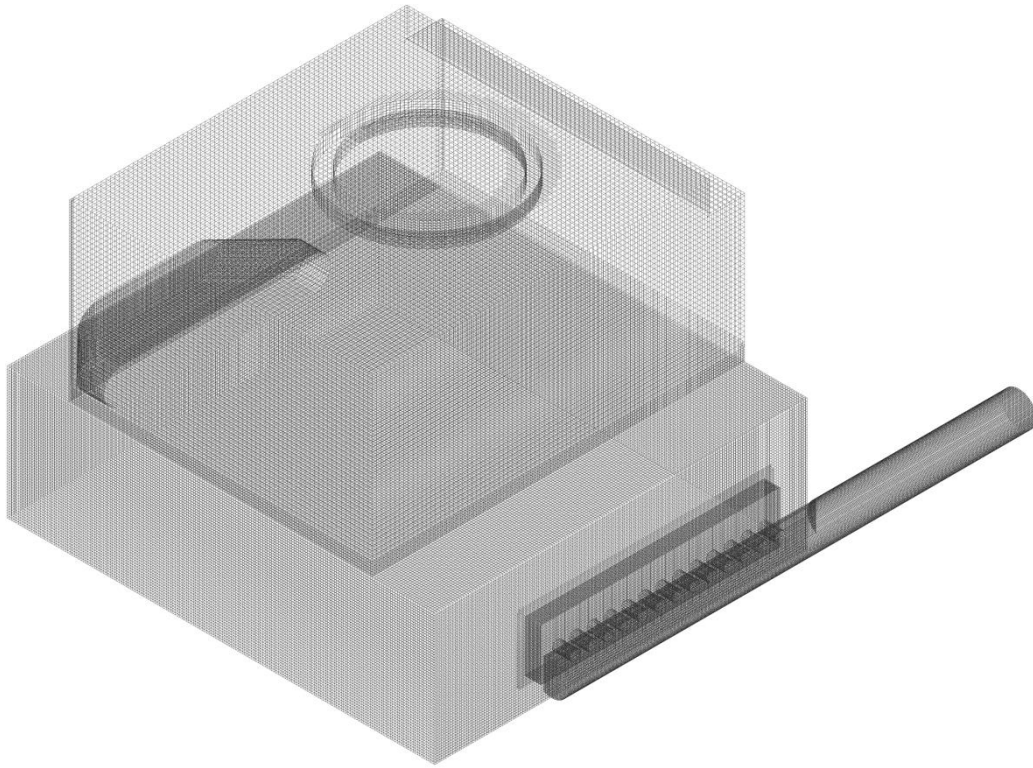
Figure 4: 3D shell mesh used for simulations

3.3 Solver

To couple the momentum and pressure equations a SIMPLE (Semi-Implicit Method for Pressure Linked Equations) algorithm was used. A solution was considered converged when continuity and momentum reach $1x10^{-4}$.

3.4 Validation of simulation against experimental results

Simulations were compared with HWA results as a guide for the most accurate computational model. The results served as a baseline model for comparison when optimisation runs are considered. Contour plot comparisons for the centre plane and the plane directly above the base plate are shown in Figure 5, where the locations of the planes are outlined in Figure 3.
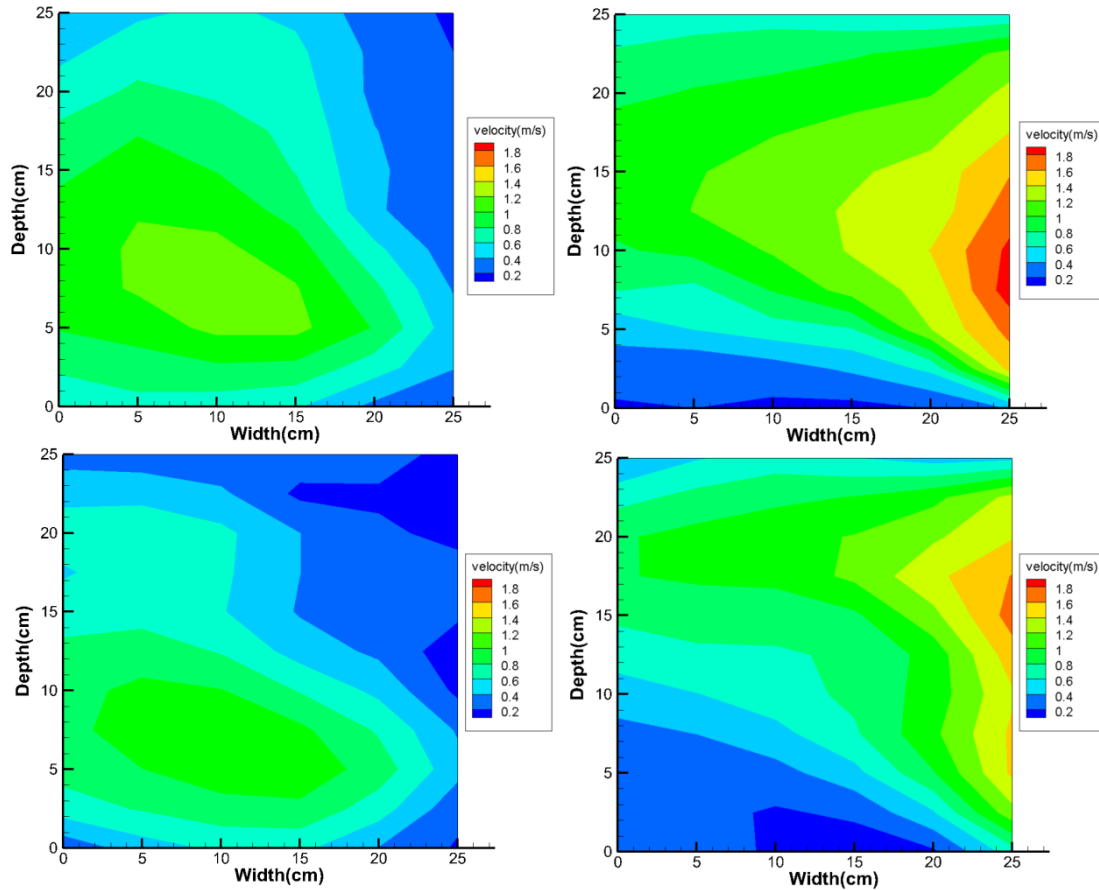
Figure 5: Experimental (HWA) against simulation (CFD) results for base plate and centre plane; top-left HWA base plate, top-right HWA centre plane, bottom-left CFD base plate and bottom-right CFD centre plane

The velocity distributions over the powder-bed and normal to the inlets are comparable with the experimental results, and accurately capture the general trend of the flow. In addition, to check that the simulations were reproducible and that they converged, the area-weighted uniformity index and the average surface facet velocity were monitored. There are some slight discrepancies between CFD and HWA readings which is most likely due to the hopper at the back of the machine not being modelled but was present during experiments. However, for practical engineering purposes these differences are considered negligible with respect to their effect on the overall flow and do not affect the important predictions of the model.

4. Discrete particle phase model

To evaluate the spatter accumulation within the build chamber which is being expelled into from the processing area a Discrete Phase Model (DPM) was developed and coupled with the argon fluid phase. Instead of re-producing the complex physical fluid flow at the melt pool level an experimental analysis of the spatter particles via high speed imaging has been undertaken. Experimental values are then imported directly into the discrete phase model in

ANSYS Fluent and coupled with the continuous argon phase model. The purpose of the work is to understand what areas the particles will be accumulating within the processing area and build chamber and how they can be mitigated using the argon gas flow.

A FASTCAM SA4 500K-M1 high speed imaging camera was used to capture the locations of spatter particles for a single line experimental build using stainless steel 316L powder. The resolution of each images was 1024 x 640 at 3600 frames per second. The Photron FASTCAM software was then used to optimise the images so that particles could most clearly be distinguished for analysis of particle trajectories using the Mosaic ImageJ particle tracking software [16]. An in-house matlab script coupled with the Mosaic ImageJ particle tracking software was developed to analyse the approximate spatter velocities. This gave a distribution of particle velocities which was then imported into the DPM via a user defined function. An example of particle identification and recorded trajectories is shown in Figure 6.
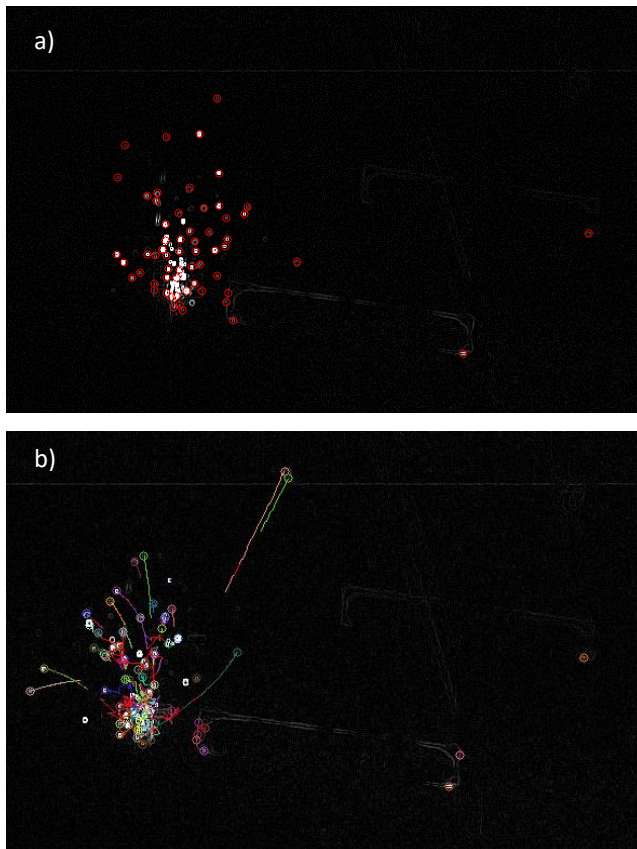

Figure 6: Particle identification and recorded trajectories analysis of high speed imaging data. a) Particle identification b) particle tracking

Particle sizes were analysed using a Malvern Mastersizer of oversized sieved powder where sizes ranged from 60-120 μm with an average of 90 μm for 316L stainless steel. Liu et.al. [11] used Energy-dispersive X-ray Spectroscopy (EDS) and found that the composition of these oversized powder particles included a higher content of oxygen in comparison to the initial fresh powder and a built SLM part but shared a very similar composition. For the DPM model the thermal physical properties of the spatter particles were set as standard stainless steel 316L.

From experimental analyses the spatter size, composition and velocity have been sufficiently approximated and inputted into the discrete phase model. A user defined function

was incorporated within the DPM to allow for a random particle release based on the statistical distribution of velocities analysed.

Model assumptions:

- Particle-particle interactions are neglected.

- Particles are spherical and non-reacting.

- Particle trajectories are pseudo random where no incorporation of biased particle trajectory based on speed or direction of the laser is included.

- Two-way coupling between continuous and discrete phase. This is required for monitoring particle accretion and concentration on boundaries.

The combination of both phases allows for the prediction of the particle accumulation rate within the processing area and what proportion of spatter will effectively be removed via the outlet port.

5. Deign exploration study

A study into the effects of simple design changes based on the current AM250 inlet rail design was undertaken. In addition, the local height of the inlet and outlet ports were varied to find an optimal height. The following input parameters were explored:

- Inlet rail diameter.
- Inlet diameters.
- Inlet and outlet height.

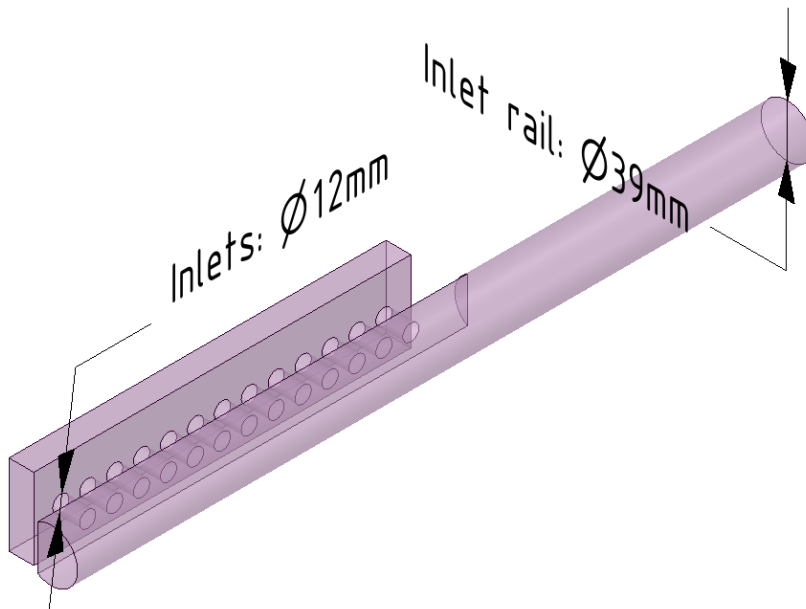The inlet rail diameter and inlet diameters are outlined in Figure 7.

Figure 7: Outline of geometrical design exploration of the current AM250 inlet rail with current dimensions

An optimal space filing algorithm was used to create 30 design points to analyse the effect of coupling input parameters to output parameters. The inlet rail radius design space was set to 15.25-29.75 mm and the inlet radii were set to 3.10-8.90 mm. Lowering of the inlet corresponds to lowering the base of the inlet manifold. The current configuration has the base of the inlet, parallel to the base plate, at 37.50 mm above the base plate. Lowering to a height of 0.00 mm indicates that the base of the inlet is at the level of the base plate. Lowering of the outlet port is in direct correlation with lowering of the inlet.

6. Results

To evaluate the results of each of the design points, the velocity magnitude directly above the base plate was evaluated. For comparison of uniformity of the flow at a plane the area-weighted uniformity index, which gives a statistical measure of the gas flow distribution of each design point is presented. Due to the varying local fluid flow velocities of each design point this allows for a non-dimensional analysis of uniformity where a value of 1 indicates the highest level of uniformity. The area-weighted uniformity index, γ for a field variable, ϕ is given as follows:

$$\gamma = 1 - \frac{\sum_{i=1}^{n}\left[\left(\left|\phi_i - \overline{\phi_a}\right|A_i\right)\right]}{2\left|\overline{\phi_a}\right|\sum_{i=1}^{n}A_i} \tag{4}$$

Where i is the facet index of a surface, A with n facets, and $\overline{\phi_a}$ is the average value of the field variable over the surface:

$$\overline{\phi_a} = \frac{\sum_{i=1}^{n}\phi_a A_i}{\sum_{i=1}^{n}A_i} \tag{5}$$

The area-weighted uniformity index of the velocity magnitude, γ was evaluated for each design point. It was previously noted that a certain minimum velocity over the powder bed is thought to be needed to effectively remove by-products from the build platform because of this the average velocity over the processing area was also evaluated as an output parameter. Finally concentrations of spatter particulates were evaluated over the processing area, all other walls within the build chamber and escaped particles.

6.1 Spearman-Rank Order correlations

The aim of the DOE was to understand the effects of the input parameters on the output parameters. The statistical sensitivities are based on the Spearman-Rank order Correlation coefficients which take into account the amount by which the output parameter varies as well as the variation of an input parameter. Positive sensitivity occurs when increasing the input increases the output. Negative sensitivity occurs when increasing the input decreases the output. Figure 8 shows the results for the DOE study conducted.
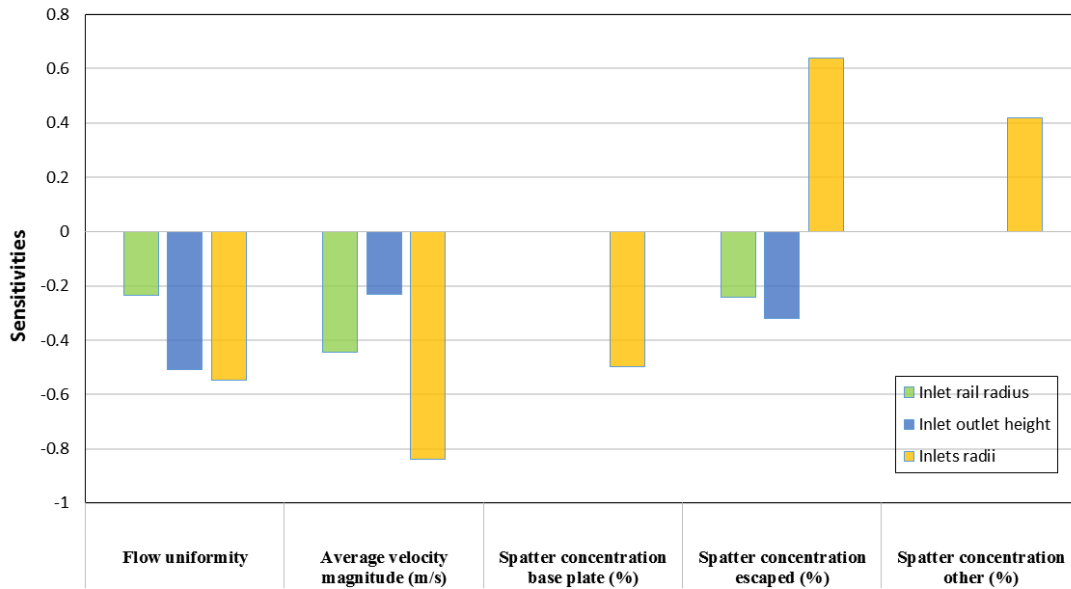
Figure 8: Spearman-Rank Order Correlation coefficients comparing effect of input parameters to output parameters

From the results it can be seen that by increasing the inlet rail radius has a slight negative effect on the flow uniformity and a slightly stronger effect on average flow velocity. Increasing the inlet rail radius negatively effects the amount of spatter removed from the build chamber.

Increasing the inlet radii has a negative effect on flow uniformity and a strong negative affect on the average flow velocity. In addition, by increasing the inlet radii it reduces the concentration of spatter on the processing area whilst increasing the spatter which escapes through the outlet port and also on all other walls. From this the main priority would be to remove spatter on the processing area but it is also favourable to increase flow uniformity.

Increasing the height of the inlet and outlet ports reduces flow uniformity whilst also slightly increasing the local flow velocity. Increasing the inlet and outlet height also slightly reduces the amount of spatter removed via the outlet.

These results were then used to guide a proposed new inlet design to more effectively remove spatter and improve flow uniformity which is important for homogeneity within a build. The proposed new designs decreased the inlet rail radius and lower the inlet and outlet ports flush with the base plate height. The inlets designs including sizes have been varied.

6.4 Initial new inlet designs

From the DOE results four proposed inlet designs have been tested to see their improvement on output parameters. They all include a reduced inlet rail radius and also lowering the inlets and outlet. It was indefinite as to whether increasing or decreasing the inlets radii will be beneficial or not. Therefore, a mixture of inlets sizes and shapes have been explored.

Design 1: Large circular radii.

Design 2: Small circular radii.

Design 3: Oval inlet design 1.

Design 4: Oval inlet design 2.

The following table outlines the designs effect on output parameters.

Table 2: Effect of new inlet design on output parameters

	Flow uniformity	Average velocity over base plate (m/s)	Spatter concentration on base plate (%)	Spatter concentration escaped (%)	Spatter concentration on other walls (%)
Original:	0.76	0.60	37.01	5.11	57.88
Design 1:	0.72	1.17	25.22	2.30	72.48
Design 2:	0.93	1.32	34.47	2.00	63.53
Design 3:	0.92	1.68	27.15	6.31	66.52
Design 4:	0.94	1.53	32.30	3.17	64.50

From these tested results design 3 gives the best improvements on output parameters. A flow uniformity increase of 21.05% and 26.64% reduction of spatter on the build platform. It also appears as if the spatter is not being removed via the outlet port but deposited in other regions of the chamber. It is noted that this could include the walls of the outlet port through the way the outlet is defined. Ideally the spatter would be removed via the outlet port but less being deposited on the processing area is ideal.

Figure 9 highlights the differences between particle accumulation of the original design and design 3. It shows that more particles are being deposited towards the outlet back wall. This demonstrates the spatter being removed from the processing area but not being directly taken out through the outlet port.
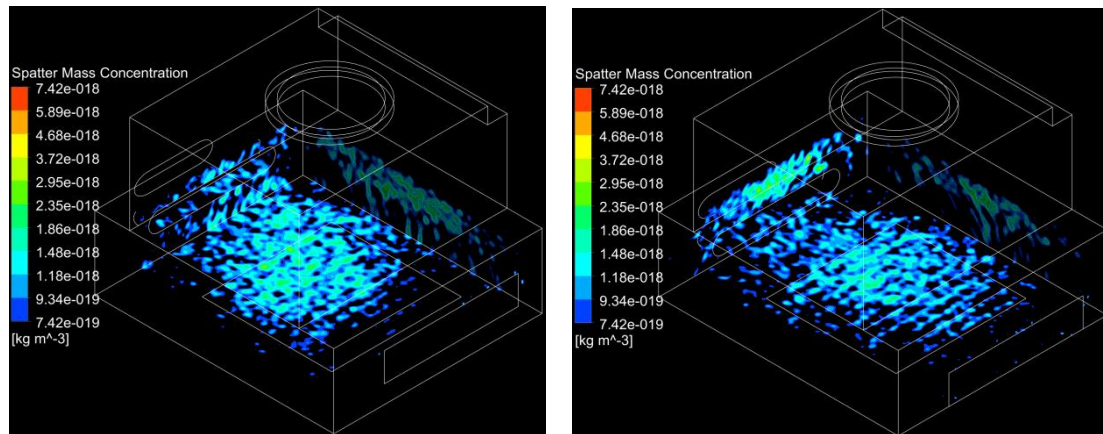

Figure 9: Comparison of spatter particle concentration for the original inlet design and design 3

6.5 Discussion

The flow uniformity and average velocity appear to be a function of inlet design and height, which is to be expected. However, the removal of spatter particulates remains unclear. Where the results imply that a higher local velocity does not directly correlate to the removal of spatter particulates from the processing area. This could potentially be down to a re-circulation zone forming within the chamber and that the particles escape the bulk flow due to their initial velocities. The recirculation zone of the argon flow could trap particulates within the machine and not effectively remove them from the build chamber and deposit in other area of the build chamber. Unfortunately the recirculation zone cannot be quantified in an effective manner. These spatter particulates may have been taken away from the process area but may not have effectively been removed from the system via the outlet. The problem is when such particulates agglomerate around the lens area of the chamber causing similar effects to laser attenuation but at larger length scales. Figure 10 shows 3D fluid flow velocity magnitudes for the original design, design 1, 2 and 3. From observation of the original design a re-circulation zone can reach the height of the lens. For designs 1 and 2 this re-circulation zone is still present yet does not reach the height of the lens. Design 3 was deemed most improved from the initial analysis. However, this re-circulation zone still reaches the height of the lens. Design 1 also performed well in reducing the amount of spatter deposited on the processing zone and it can be observed that the re-circulation zone is reduced.
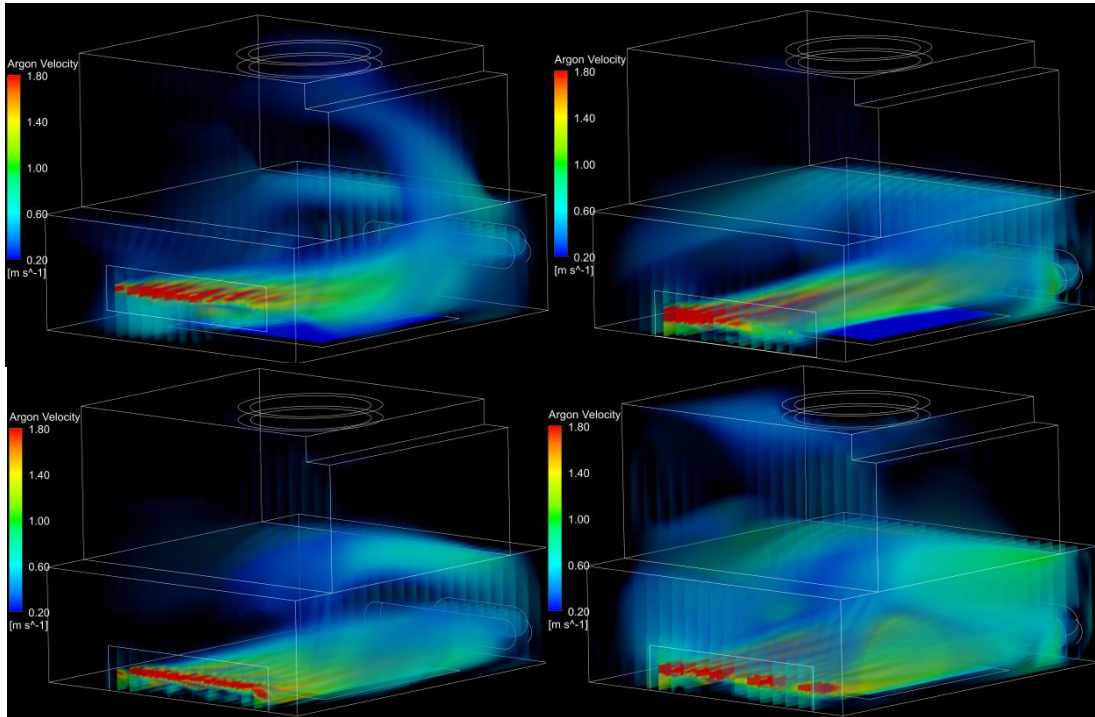

Figure 10: Volume rendering of fluid flow velocity magnitude. a) Original b) design 1 c) design 2 d) design 3.

7. Conclusions

The Renishaw AM250 metal powder bed fusion's gas flow system has been modelled using CFD. This model has been validated using HWA readings of the gas flow regime. In addition, this CFD model has been coupled with a DPM for prediction of spatter particulate accumulation.

A DOE study was performed to understand the key design parameters which effected the defined output parameters. It was found that reducing the inlet rail radius had a positive effect on flow uniformity, average flow velocity and particulate removal. Reducing the inlet radii improved flow uniformity and average velocity but decreased the amount of spatter effectively being removed but reduced the amount accumulated on the processing area. Also, moving the inlet and outlet height flush with the processing area improved flow uniformity, increased local fluid velocity and also removed slightly more spatter particulates through the outlet.

From this the DOE highlighted the important factors which could improve output parameters, where four new proposed inlet designs were tested. It was found that an increase of 21.05% of flow uniformity and a reduction of 26.64% of spatter accumulation on the processing area could be achieved. However, the re-circulation zone which is not desirable within the machine was reduced but not completely removed for this proposed design. The removal of spatter particulates ideally needs to be removed in its entirety so further design iterations will be tested.

Future work will carry on this initial design study to further improve the inlet manifold design and to gain further insight into design parameters for future generation machines.

References

[1]   S. Das, "Physical Aspects of Process Control in Selective Laser Sintering of Metals," *Advanced Engineering Materials*, vol. 5, no. 10, pp. 701–711, 2003.

[2]   W. E. King, A. T. Anderson, R. M. Ferencz, N. E. Hodge, C. Kamath, S. A. Khairallah, and A. M. Rubenchik, "Laser powder bed fusion additive manufacturing of metals; physics, computational, and materials challenges," *Applied Physics Reviews*, vol. 2, no. 4, p. 41304, 2015.

[3]   C. H. Fu and Y. B. Guo, "Three-Dimensional Temperature Gradient Mechanism in Selective Laser Melting of Ti-6Al-4V," *Journal of Manufacturing Science and Engineering*, vol. 136, no. 6, p. 61004, 2014.

[4]   C. Körner, E. Attar, and P. Heinl, "Mesoscopic simulation of selective beam melting processes," *Journal of Materials Processing Technology*, vol. 211, no. 6, pp. 978–987, 2011.

[5]   S. A. Khairallah, A. T. Anderson, A. Rubenchik, and W. E. King, "Laser powder-bed fusion additive manufacturing: Physics of complex melt flow and formation mechanisms of pores, spatter, and denudation zones," *Acta Materialia*, vol. 108, pp. 36–45, 2016.

[6]   Y. S. Lee and W. Zhang, "Modeling of heat transfer, fluid flow and solidification microstructure of nickel-base superalloy fabricated by laser powder bed fusion," *Additive Manufacturing*, 2016.

[7]   H. W. Mindt, M. Megahed, N. P. Lavery, M. A. Holmes, and S. G. R. Brown, "Powder Bed Layer Characteristics: The Overseen First-Order Process Input," *Metallurgical and Materials Transactions A: Physical Metallurgy and Materials Science*, vol. 47, no. 8, pp. 1–12, 2016.

[8]   A. Hussein, L. Hao, C. Yan, and R. Everson, "Finite element simulation of the temperature and stress fields in single layers built without-support in selective laser melting," *Materials and Design*, vol. 52, pp. 638–647, 2013.

[9]   I. A. Roberts, C. J. Wang, R. Esterlein, M. Stanford, and D. J. Mynors, "A three-dimensional finite element analysis of the temperature field during laser melting of metal powders in additive layer manufacturing," *International Journal of Machine Tools and Manufacture*, vol. 49, no. 12–13, pp. 916–923, 2009.

[10]   A. Ladewig, G. Schlick, M. Fisser, V. Schulze, and U. Glatzel, "Influence of the shielding gas flow on the removal of process by-products in the selective laser melting process," *Additive Manufacturing*, vol. 10, pp. 1–9, 2016.

[11]   Y. Liu, Y. Yang, S. Mai, D. Wang, and C. Song, "Investigation into spatter behavior during selective laser melting of AISI 316L stainless steel powder," *Materials and Design*, vol. 87, pp. 797–806, 2015.

[12]   B. Ferrar, L. Mullen, E. Jones, R. Stamp, and C. J. Sutcliffe, "Gas flow effects on selective laser melting (SLM) manufacturing performance," *Journal of Materials Processing Technology*, vol. 212, no. 2, pp. 355–364, 2012.

[13]   J. Ding, P. Colegrove, F. Martina, S. Williams, R. Wiktorowicz, and M. R. Palt, "Development of a laminar flow local shielding device for wire+arc additive manufacture," *Journal of Materials Processing Technology*, vol. 226, pp. 99–105, 2015.

[14]   A. Masmoudi, R. Bolot, and C. Coddet, "Investigation of the laser–powder–atmosphere interaction zone during the selective laser melting process," *Journal of Materials Processing Technology*, vol. 225, pp. 122–132, 2015.

[15]   W. L. Oberkampf and T. G. Trucano, *Verification and validation in computational fluid dynamics*, vol. 38, no. 3. 2002.

[16]   I. F. Sbalzarini and P. Koumoutsakos, "Feature point tracking and trajectory analysis for video imaging in cell biology," *Journal of Structural Biology*, vol. 151, no. 2, pp. 182–195, 2005.